Stigmatic imaging of secondary ions in MeV-SIMS spectrometry by linear Time-of-Flight mass spectrometer and the TimePix detector

Nuclear Inst. and Methods in Physics Research B 452 (2019) 1–6

Contents lists available at ScienceDirect

Nuclear Inst. and Methods in Physics Research B

journal homepage: www.elsevier.com/locate/nimb

Stigmatic imaging of secondary ions in MeV-SIMS spectrometry by linear Time-of-Flight mass spectrometer and the TimePix detector

Boštjan Jenčič[a,*], Luka Šepec[a], Primož Vavpetič[a], Mitja Kelemen[a], Zdravko Rupnik[a], Matjaž Vencelj[a], Katarina Vogel-Mikuš[a,b], Nina Ogrinc Potočnik[c], Shane R. Ellis[c], Ron M.A. Heeren[c], Primož Pelicon[a]

[a] Jožef Stefan Institute, Jamova 39, SI-1000 Ljubljana, Slovenia
[b] University of Ljubljana, Biotechnical Faculty, Dept. of Biology, Večna pot 11, SI-1000 Ljubljana, Slovenia
[c] The Maastricht Multimodal Molecular Imaging Institute (M4I), Division of Imaging Mass Spectrometry, Maastricht University, 6229 ER Maastricht, The Netherlands

ARTICLE INFO

Keywords:
MeV-SIMS
Stigmatic imaging
Time-of-Flight

ABSTRACT

Secondary ion mass spectrometry (SIMS), based on primary ions within the MeV energy domain, also known as MeV-SIMS, is a subject of increasing scientific interest. The main drive for the interest in the development of MeV-SIMS is the ability to desorb high yields of large non-fragmented organic molecular ions from the sample surface. This makes MeV-SIMS particulary useful in imaging of biological tissues.

Imaging methods based on scanning a focused primary ion beam are associated with demanding focusing of the heavy energetic ions. As an alternative, stigmatic imaging mode has been studied here, applying point-to-point imaging characteristics of secondary ions in the linear Time-Of-Flight mass spectrometer. In stigmatic imaging approaches, spatial resolution is independent of the focussed spot size of the ionising primary ion beam, but instead dependant on the ability of the ion optics to project an image of the ion distributions removed from the surface onto a position sensitive ion detector.

1. Introduction

Molecular imaging plays an important role in biomedical research, providing both identification and lateral distribution of molecules in living organisms [1–4]. Molecular imaging is frequently applied to study the drug metabolism in pharmaceutical research [5–8], as well as plant [9,10], animal [11] and human physiology [12,13].

Among the techniques of Mass Spectroscopy Imaging (MSI), the Secondary Ion Mass Spectrometry [14,15] with high-energy heavy (swift) ions (MeV-SIMS) [16] is emerging as a novel tool for molecular imaging at intact, chemically non-processed sections of biological materials. In contrast with the conventional Secondary Ion Mass Spectrometry (SIMS), which uses atomic or cluster ions with energies ranging between 0.5 and 30 keV, it provides significantly higher yields of non-fragmented ionised species [17,18]. Secondary ions are in this case formed in a specific desorption process, induced by the collision of heavy ion with the energy in the MeV range (swift ion) with insulating material, governed by electron stopping processes instead of nuclear collisions. Specific characteristics of MeV-SIMS offer analytical possibilities in cases where other MSI techniques such as SIMS, DESI (Desorption electrospray ionisation) [19] and MALDI (Matrix-assisted laser desorption ionization) [20–22] experience difficulties, linked to low high-mass molecular yields (i.e. SIMS), specific surface preparation, or low lateral resolution (DESI, MALDI). The development of MeV-SIMS technique at Jožef Stefan Institute (JSI) [23,24] was motivated as a complementary chemical imaging method to elemental imaging with micro-PIXE [25–27]. For the MeV-SIMS technique, a 2 MV tandetron accelerator [28] is used to accelerate ^{35}Cl ions having charge states of 5+, 6+ and 7+, to corresponding energies between 5 and 12 MeV. The energy and charge of the primary ion beam are customized by the needs of the research, with lower energy ions favouring tighter beam focusing and enabling higher lateral resolution, while higher energy ions being used, when higher yields of non-fragmented heavier molecular ions (i.e. m/Z > 1000 Da) are desired. The most commonly used ions for the molecular imaging with MeV-SIMS at JSI are $^{35}Cl^{6+}$ with energy of 5.8 MeV.

Currently, there are two modes of MeV-SIMS in operation at JSI. The pulsed beam mode of MeV-SIMS operation is using a pulsed primary ion beam, which bombards the sample residing in a vacuum of about 5×10^{-7} mbar. The sputtering process then desorbs the

* Corresponding author.
E-mail address: bostjan.jencic@ijs.si (B. Jenčič).

https://doi.org/10.1016/j.nimb.2019.05.040
Received 30 July 2018; Accepted 14 May 2019
Available online 23 May 2019
0168-583X/

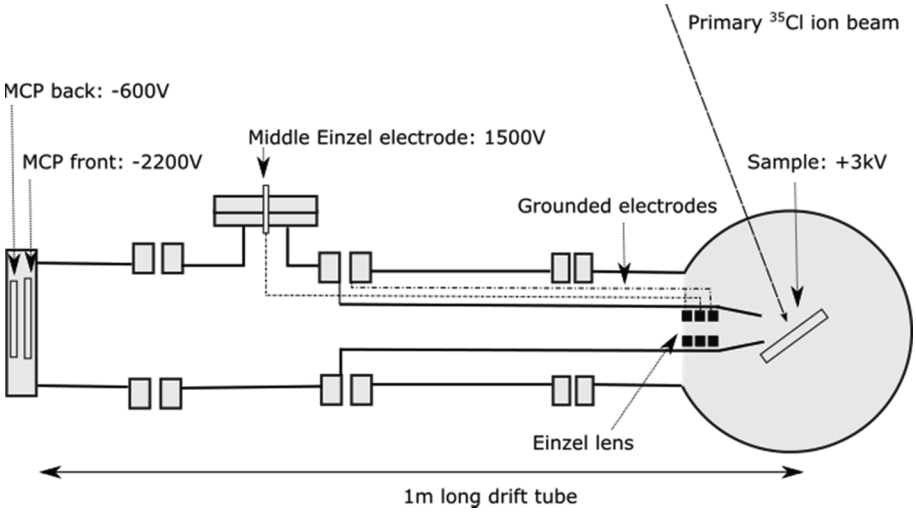

Fig. 1. Scheme of a mass spectrometer at JSI.

secondary ions from the sample, which are extracted into the 1 m long drift tube with an MCP detector at the end by the extraction voltage of several kV (Fig. 1).

Time of flight (ToF) of desorbed molecules measures the time elapsed between the primary ion strike onto the sample and the signal recorded at the MCP detector. The ToF is then used to calculate the mass-to charge (m/z) values of the ionised secondary molecules. The primary beam is pulsed with a parallel plate deflector, positioned in the direction of the beam, 7 m upstream from the sample. One of the plates of the deflector is constantly biased at 900 V, and the other is switching from 0 to 900 V for short duration, i.e. 30 ns. The frequency of such pulses is 10 kHz, which results in a poor duty factor of less than 0.1%. Therefore, the need to achieve relevant counting statistics dictates wide opening of microprobe forming slits, which results in a moderate primary beam size enabling the lateral resolution of typically $15 \times 15\,\mu m^2$.

In the pursuit to develop mass spectroscopy imaging with sub-micrometre resolution, which would enable sub-cellular molecular imaging within single cells, we developed the alternative measuring mode using a continuous primary ion beam. In this case, a focused primary swift ion beam of approx. 5000 ions/sec is scanned over the sample (a thin biological tissue slice, suspended on a thin conductive supporting membrane). A continuous electron multiplier (CEM, channeltron) positioned behind the sample detects the arrival of each individual primary ion pulse and triggers the start signal for TOF measurement. Such technique allows us to reach sub-micron lateral resolution, as we are able to strongly reduce the sizes of the slits in the microbeam forming system. In addition, the elimination of time uncertainty related to the finite length of the primary ion pulse in the pulsed beam mode, the timing (mass) resolution of the spectra in the continuous primary beam mode is also greatly improved. As the samples should be prepared very thin (3–5 μm) to enable the penetration of the swift primary ions to the CEM detector, the continuous primary mode MeV-SIMS is not applicable on specific materials, i.e. human hair [29].

A major constraint in further improvement of the MeV-SIMS is connected with the focusing power of the quadrupole triplet, limited to the primary ion rigidity of 8 MeV amu/Z^2. The molecular yield in MeV-SIMS conditions scales approximately as the third power of the stopping power of the primary ion at the surface of the sample [30]. At 2 MV tandems, $^{35}Cl^{6+}$ ion beams could be accelerated to the energies of up to 14 MeV, a beam of potentially high quality characteristics for the MeV-SIMS. This is, however, beyond the reach to focus on our focusing beam optics, consisting of standard Oxford magnetic quadrupole triplet lens [31].

It is of potentially great interest to overcome the need to focus high-energy heavy primary ions (swift ions) for MeV-SIMS. One of the approaches allowing imaging mode of analysis without the focusing of the primary swift ions is relaying on the so-called stigmatic imaging. Stigmatic imaging is a specific property of the electrostatic cylindrically symmetric lenses to transfer charge particles originated from a distinct point in the object plane to a well-defined point in the image plane.

2. Characteristics of the einzel lens at the entrance of ToF detector

At the JSI MeV-SIMS setup, the extracted secondary ions enter the linear TOF spectrometer through an einzel lens consisting of three electrodes. The middle one can be biased to a selected voltage, while the other two are grounded. Through generation of electric field by the three electrodes, einzel lens focuses secondary ions without changing their energy. Due to the axially symmetric electric field, it is able to perform point to point focusing of secondary ions, referred to as stigmatic imaging (Fig. 2) [32,33].

The application of the einzel lens at the entrance of the TOF spectrometer drastically improves the collection efficiency of secondary ions. In general, the yield of secondary ions can be enhanced to nearly 100% collection efficiency. In addition, the application of the entrance electrostatic lens offers a convenient alternative for the focusing of the primary ion beam. Its sigmatic imaging ability allows the application of a homogeneous broad beam, which impacts the selected area of interest on the sample to enable simultaneous imaging of the entire impacted area. In this case, focusing with quadrupole lenses is avoided, which largely simplifies the hardware complexity. In addition, much higher primary ion fluxes are possible and its intensity could easily be turned to the capacity of detection system. In this case the MeV-SIMS analysis could be executed with high magnetic rigidity primary ion beams, optimal for the secondary molecular ion yields.

The theoretical calculations based on above equations, as well as calculations done by SIMION program [24], predicted the optimal bias on the einzel lens to be approx. 1300 V, which increases the yield of secondary ions for at least one order of magnitude (Fig. 3).

3. Time-Pix detector

In order to understand the trajectories of desorbed molecular ions in the spectrometer, we replaced our MCP stop detector with the TimePix secondary ion detector. TimePix detector is a fast position sensitive detector, developed [34] within the CERN hosted Medipix collaboration (www.cern.ch/medipix) and previously applied to various spectrometry applications including stigmatic imaging [35–38]. Secondary ions at the end of the flight tube of the TOF spectrometer are detected for their arrival time and position by Timepix chip positioned after a

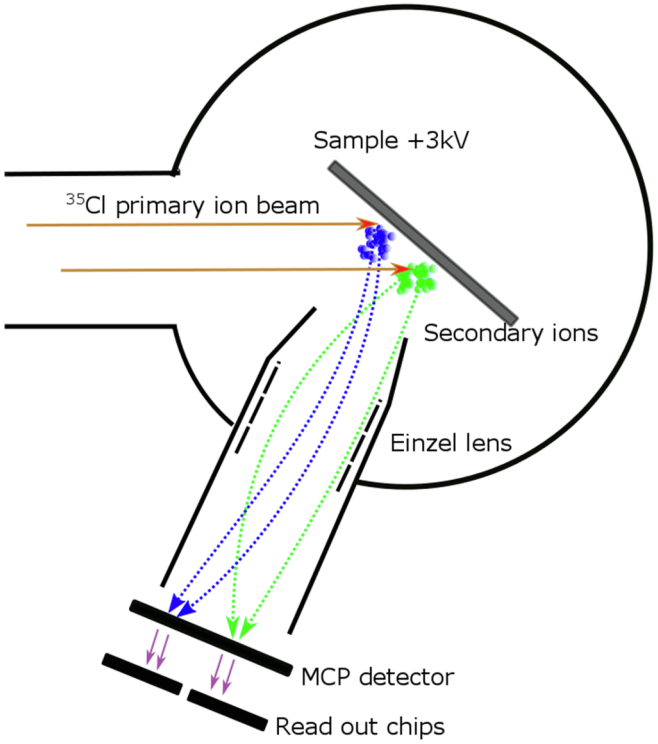

Fig. 2. Schematic figure of the MeV-SIMS setup and the stigmatic imaging of secondary ions by einzel lens. Blue and green trajectories demonstrate the translation of secondary ions to the specific 2D point on TimePix detector. (For interpretation of the references to colour in this figure legend, the reader is referred to the web version of this article.)

double-stack MCP detector. The impact of secondary ion on the MCP stack produces an electron shower, which is detected by the sensitive area of the Timepix setup positioned 2 mm behind the back MCP.

The TimePix detector consists of an array of 2 × 2 Timepix chips. Each of the four Timepix chips applied in the TimePix detector has dimension of 1.4 × 1.6 cm^2 and consists of 256 × 256 pixels. The centre-centre spacing of adjacent pixels is 55 μm. Each pixel of the Timepix chip can be individually selected to operate in one of the three different modes: 1.) the Medipix mode, where each pixel counts the number of incoming particles, 2.) the time-of-arrival mode, where the arrival of one particle is measured with respect to an external trigger/shutter signal, 3.) the time-over threshold mode, where the time is measured during which a fired pixel stays over a certain detection threshold. For the purposes of MeV-SIMS operation, we were using the time-of-arrival operation mode, where the trigger signal correlates with the arrival of the primary ion pulse.

After we successfully installed and applied the detector on the TOF mass spectrometer, we were able to gain better understanding of operation of our einzel lens and enabled us a precise *in operando* alignment. The used primary ion beam was 5.8 MeV $^{35}Cl^{6+}$, and measurements were performed on the Leucine amino acid reference sample, consisting of leucine spin–coated on a Silicon wafer the acquired spectrum is shown in Fig. 4.

The time resolution of the TimePix detector amounts 20 ns, which is rather poor for the application in ToF mass spectrometry. The detected stop pulses are significantly spread over time, thus mass resolution of acquired results was limited to m/dm = 300. Nonetheless, the low mass resolution had limited effect on our experiments, as the acquisition of high mass resolution spectra was not our primary goal. Our goal was to explore the ability of stigmatic imaging and the achievable resolution was sufficient.

4. Results

4.1. Operation of einzel lens

In the initial testing phase of the setup, the secondary ions produced at the centre of the observed sample frame, were not spatially focused at the TimePix detector, when the einzel lens was biased by the voltages, predicted by the ion optical simulations. We observed that increasing the bias of the einzel lens resulted in secondary ions impact outside the TimePix detector and were thus not recorded. With the detection system turned on (*in operando*), mechanical realignment of the TOF spectrometer consisting of iterating translations of the spectrometer axis both in vertical and horizontal direction of 100 μm, resulted in the formation of a well-defined focus in the central part of the TimePix detector (Fig. 5).

After carefully completed realignment of the TOF spectrometer, we observed the spectrometer collection efficiency as a function of einzel lens voltage. The measured collection efficiency (Fig. 4) shows a dependency on the einzel lens bias voltage well in agreement to the one obtained by theoretical simulations. In the case of sample bias voltage at 3 kV, einzel lens bias of 1500 V leads to the maximum detection efficiency.

4.2. Stigmatic imaging

The quality of stigmatic imaging was evaluated by applying a focused pulsed primary 5.8 MeV $^{35}Cl^{6+}$ beam with dimension of 15 × 15 μm^2 to the silicon wafer spin-coated by leucine.

In the first series of measurements, we parked the primary beam at the centre of the sampling frame. The integrated signal of secondary ions at the TimePix detector as a function of their position were recorded as a function of the einzel lens bias. The number of hits as a function of secondary ion position at the TimePix detector with 512 × 512 pixels are shown in Fig. 5. The distribution of the ions at the

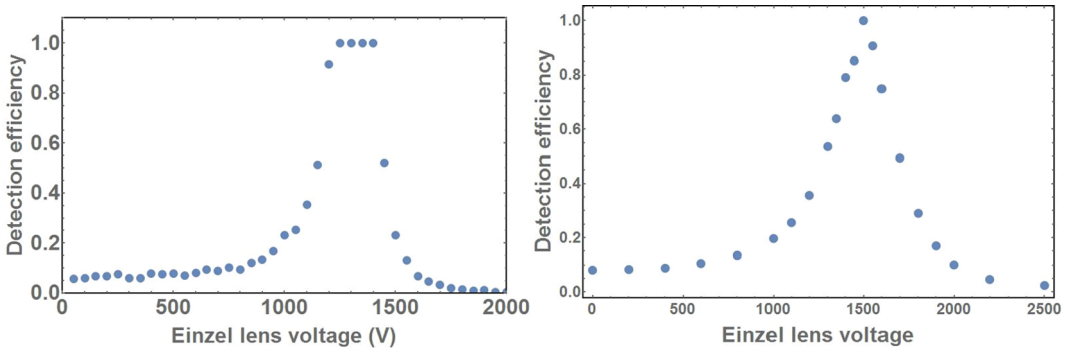

Fig. 3. Dependence of number of total counts of the MCP detector as a function of einzel lens voltage both in theory (above) and experimentally acquired (bellow). Sample bias was set to 3 kV.

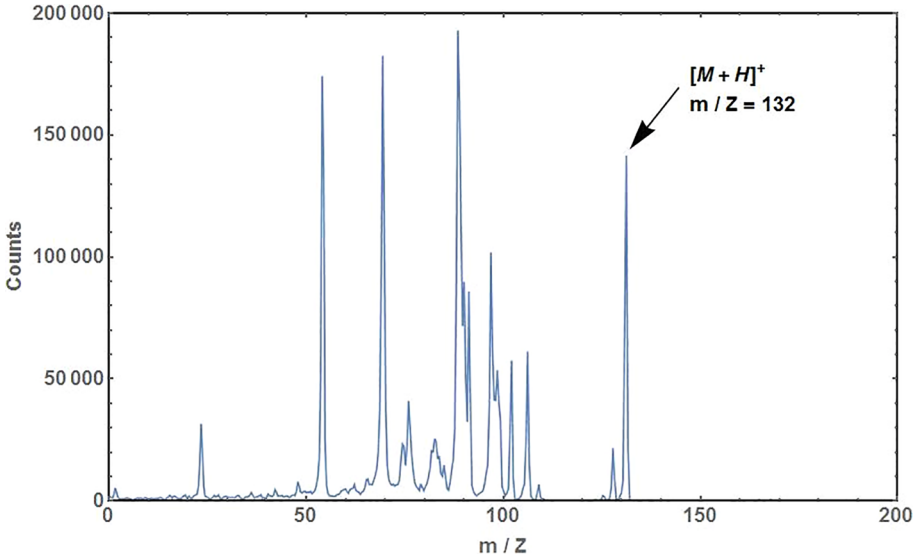

Fig. 4. Spectra of the Leucine amino-acid standard, acquired by the TimePix detector.

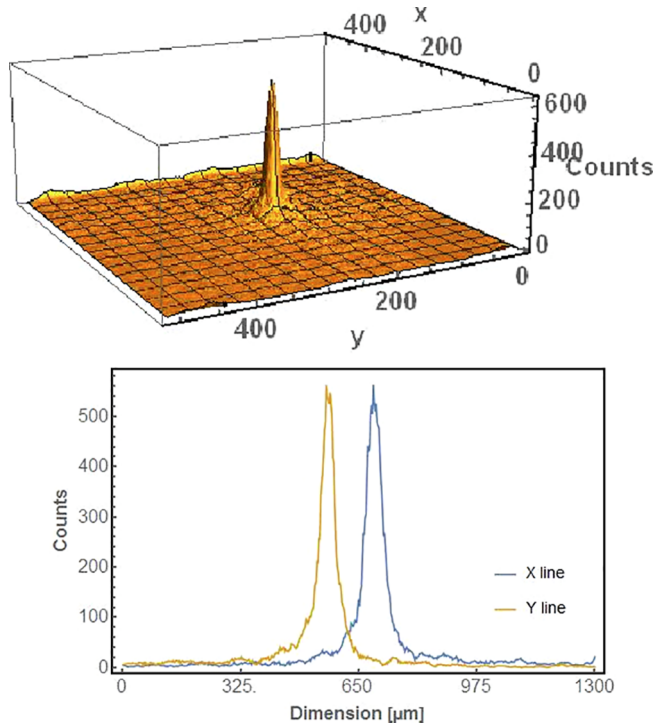

Fig. 5. Total number of Leucine $[M+H]^+$ secondary ions, detected as a function of their striking position at TimePix detector, when parking the primary ion beam at the centre of the sample frame. Ion count is shown two dimensionally (above), and in 1D (bellow). FWHM of the peak is 45 μm in horizontal and 40 μm in vertical direction. The final stigmatic imaging resolution was estimated by deconvolution of the primary ion beam diameter of 15 × 25 μm^2.

TimePix detector could be reasonably fitted with a symmetric two-dimensional gaussian function.

We observed similar behaviour when using sample biases of 1 kV, 2 kV and 4 kV, with optimal lens voltages at approximately 500 V, 1000 V and 2 kV, respectively. We also obtained similar results with negatively biased lens. The optimal einzel lens value for sample bias of −1 kV was found at approx. +1070 V. The optimal positive lens voltage therefore corresponds to approx. ½ of the sample bias, while the optimal negative voltage has its value similar to the absolute value of sample bias. All the parameters are also dependent on the position of the nozzle, which forms and shapes the field to attract the secondary molecules. The optimal sample lens distance was found at 8 mm and all the results reported here were obtained at this position.

Results show the action of the einzel lens in maximizing the yield of secondary ions. The ratio between the total secondary yields with einzel lens turned on and off is ~12, which presents the opportunity to reduce the primary beam size by a factor of about 3 without compromising sensitivity compared to the previous setup. The 5.8 MeV $^{35}Cl^{6+}$ primary ion beam was previously focused to 15 μm with respect to optimal count rate. Using the einzel lens, we can cut and focus the same beam down to 5 μm diameter or less with the same resulting counting rate at the mass spectrometer. The optimal focusing voltage does not differ significantly for the secondary ion masses ranging from 1 to 1000 Da. The lateral resolution as a function of einzel lens voltage follows the trend of detection efficiency and reaches its peak at approx. 1510 V (Fig. 6).

It is important to know, that the sample must be rotated by a polar angle of 55° in order to have its surface perpendicular to the axis of TOF spectrometer, and successfully extract and detect secondary ions. Therefore, the dimensions at the horizontal (x) axis are stretched by a factor of 1/cos(55°). The primary ion beam was scanning in transverse direction over the area of 1.3 × 1.3 mm^2, thus the effective scanned area over the tilted sample was 1.3 × 2.3 mm^2. Since the axis of the mass spectrometer is aligned with the normal of the sample plane, the

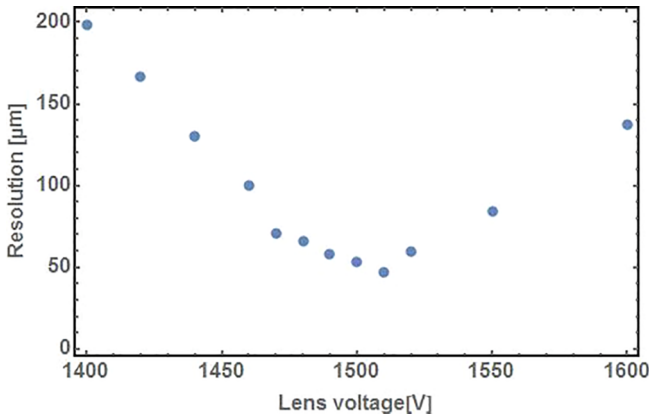

Fig. 6. Lateral resolution (FWHM) of secondary ions on the MCP detector as a function of einzel lens voltage. Optimum is found at 1510 V, which corresponds to the optimal voltage for highest total ion yield.

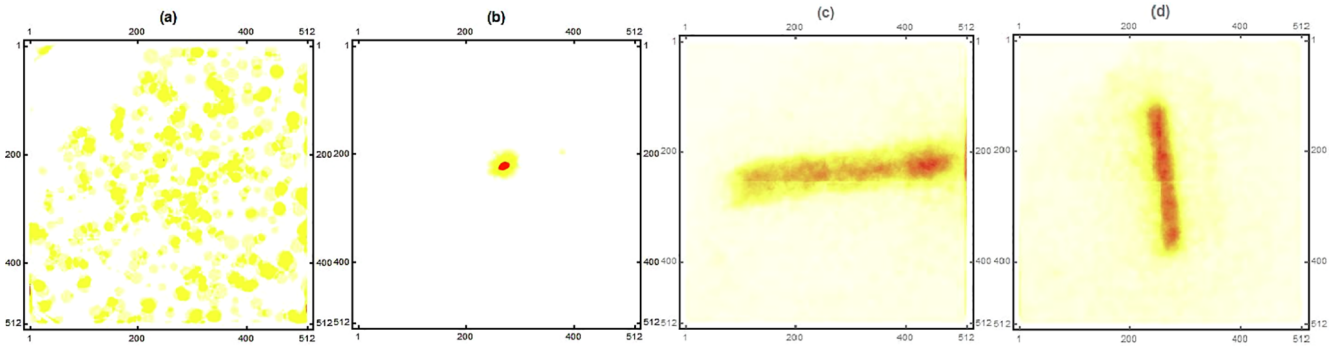

Fig. 7. Position dependent total counts of secondary ions on MCP detector when irradiating the centre spot of the sample without (a) and with (b) einzel lens, when scanning the full horizontal (c) and vertical (d) line over the sample.

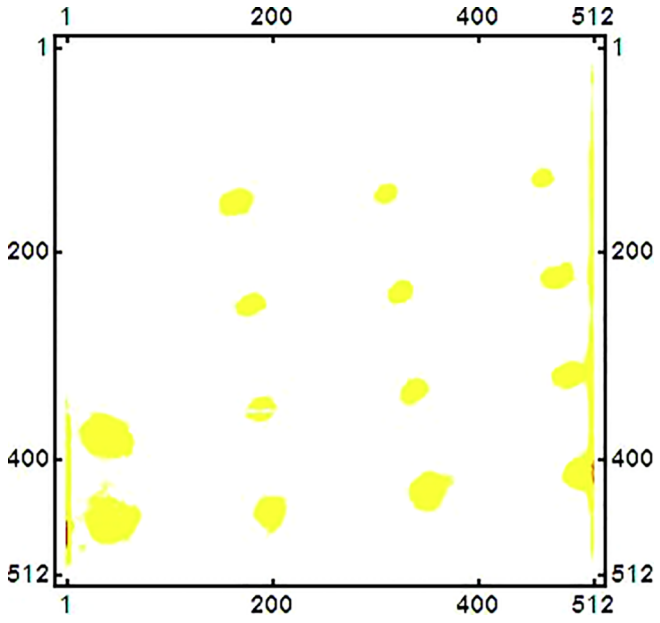

Fig. 8. Matrix of total number of secondary ions originating from matrix of points at the sample. The resolution is highly impacted from horizontal shift and less from the vertical shift off the main axis.

transformation of the x axis is visible on a detector, and the scanned area corresponds to 256 × 450 pixels on the detector. One pixel with a size of 55 × 55 μm^2 therefore represents area of 5.0 × 5.0 μm^2 on the sample.

First tests with the focused primary ion beam proved the stigmatic ability of the linear TOF mass spectrometer, equipped with the entrance einzel lens. The horizontal, vertical and full scans over the Leucine amino-acid sample desorbed molecules from the distinct arrays of points aligned along the vertical or horizontal axis. This reflects in the impact coordinates of the secondary ions to the TimePix detector (Fig. 7).

FWHM of the peak at Fig. 5 is 45 μm in horizontal and 40 μm in the vertical direction. We estimated the final stigmatic imaging resolution by deconvolution of the primary ion beam size at the sample of 15 × 25 μm^2. This yields a final resolution of the stigmatic imaging process of 37 × 37 μm^2.

The estimated resolution of the stigmatic imaging of 40 μm is only valid for secondary ions, which are desorbed near central axis of the mass spectrometer. The horizontal and vertical line scans over the samples already suggest, that the imaging resolution of the secondary ions worsens, as their starting point departures significantly from the optical axis of the system due to the aberration effects on the einzel lens optics. To investigate this effect we performed a series of generated 4x4 matrices in order to obtain an insight into the resolution behaviour as a function of distance from the axis (Fig. 8). The results show the influence of the distance from the central axis. The resolution on the far right edge at the centre of the vertical axis worsens to a value of 75 μm, and the resolution on the lower edge at the centre of the horizontal axis to a value of 60 μm. At the corner of the full scan rectangle, the resolution worsens to values above 100 μm. The stigmatic imaging resolution degrades with increasing axial distance from the optical axis, as expected from the axial symmetry of the einzel lens.

5. Conclusion

The application of the two-dimensional position sensitive detector with fast time ability (TimePix) enabled us a valuable insight in the operation of the linear Time-Of-Flight mass spectrometer. The properties of einzel lens were investigated with respect to operational parameters and alignment of the spectrometer conveyed *in operandi* and the possibility of performing stigmatic imaging with MeV-SIMS was experimentally investigated. The results show, that stigmatic imaging could be a valuable asset for a fast molecular mapping with modest lateral resolution of 37 μm, as it eliminates the demand of point to point scanning. After preliminary attempts to chemically map plant tissue slices on silicon wafer, it became clear that this type of imaging is extremely sensitive to sample tomography and minute local charging in comparison to the imaging with a scanning focused beam.

The testing results obtained on reference materials spun over the silicon wafer indicate that thin and flat tissue slices with metallized surface layer may be a subject of successfull MeV-SIMS molecular imaging with broad primary beam, combining stigmatic imaging property of collecting electrostatic lens, and position sensitive detection with fast timing resolution.

References

[1] R. Caprioli, Molecular imaging of tissue sections by mass spectrometry: looking beyond the microscope, J. Biomol. Tech. 23 (2012) 58.
[2] C.N. Ferguson, J.M. Fowler, J.F. Waxer, R.A. Gatti, J.A. Loo, Mass spectrometry – based tissue imaging of small molecules, Adv. Exp. Med. Biol. 806 (2014) 283–299.
[3] J. Soltwisch, H. Kettling, S. Vens-Capell, M. Wiegelmann, J. Muthing, K. Dreisewerd, Mass spectrometry imaging with laser – induced postionization, Science 348 (2015) 211–215.
[4] A. Bodzon-Kulakowska, P. Suder, Imaging mass spectrometry: Instrumentation, applications and combination with other visualization techniques, Mass. Spectr. Rev. 35 (2016) 147–169.
[5] B. Prideaux, M. Stoeckli, Mass spectrometry imaging for drug distribution studies, J. Proteomics 75 (2012) 4999–5013.
[6] Y.S. Zhao, C. Li, Mass spectrometry imaging: applications in drug distribution studies, Curr. Drug Metab. 16 (2015) 807–815.
[7] S. Giordano, M. Zucchetti, A. Decio, M. Cesca, I. Fuso Nerini, M. Maiezza, M. Ferrari, S.A. Licandro, R. Frapolli, R. Giavazzi, D. Maurizio, E. Davoli, L. Morosi, Heterogeneity of paclitaxel distribution in different tumor models assessed by MALDI mass spectrometry imaging, Sci. Rep. 6 (2016) 39284.
[8] E. Patel, MALDI – MS imaging for the study of tissue pharmacodynamics and toxicodynamics, Bioanalysis 7 (2015) 91–101.

[9] N. Bjarnholt, B. Li, J. D'Alvise, C. Janfelt, Mass Spectrometry imaging of plant metabolites – principles and possibilities, Nat. Prod. Rep. 31 (2014) 818–837.
[10] Y. Dong, B. Li, S. Malitsky, I. Rogachev, A. Aharoni, F. Kaftan, A. Svatoš, P. Franceschi, Sample preparation for mass spectrometry imaging of plant tissues: a review, Front. Plant Sci. 7 (2016) 60.
[11] J.D. DeBord, D.F. Smith, C.R. Anderton, R.A. Heeren, L. Paša-Tolić, R.H. Gomer, F.A. Fernandez-Lima, Secondary ion mass spectrometry imaging of Dictyostelium dilcoideum aggregation streams, PLoS One (2014) e99319.
[12] D.C. Barbacci, A. Roux, L. Muller, S.N. Jackson, J. Post, K. Baldwin, B. Hoffer, C.D. Balaban, J.A. Schultz, S. Gouty, B.M. Cox, A.S. Woods, Mass spectrometric imaging of ceramide biomarkers tracks therapeutic response in traumatic brain injury, ACS Chem. Neurosci. 8 (10) (2017) 2266–2274, https://doi.org/10.1021/acschemneuro.7b00189.
[13] M. Angelo, C. Sean, S.C. Bendall, R. Finck, M.B. Hale, C. Hitzman, A.D. Borowsky, R.M. Levenson, J.B. Lowe, S.D. Liu, S. Zhao, Y. Natkunam, G.P. Nolan, Multiplexed ion beam imaging of human breast tumors, Nat. Med. 20 (2014) 436–442.
[14] J.C. Wickerman, I. Gilmore, Surface Analysis: The Principal Techniques, second ed., Wiley, 2009.
[15] T.L. Alford, L.C. Feldman, J.W. Mayer, Fundamentals of Nanoscale Film Analysis, Springer, 2007.
[16] Y. Nakata, Y. Honda, S. Ninomiya, T. Seki, T. Aoki, J. Matsuo, Matrix-free high-resolution imaging mass spectrometry with high-energy ion projectiles, J. Mass Spectrom. 44 (2009) 128–136.
[17] A. Hedin, P. Hakansson, B. Sundqvist, Phys. Rev. B 31 (1985) 1780–1787.
[18] P. Sigmund, Fundamental Processes in Sputtering of Atoms and Molecules, Copenhagen, 1993.
[19] Z. Takats, J.M. Wiseman, B. Gologan, G. Cooks, Science 306 (2004) 471–473.
[20] J.C. Wickerman, Analyst 136 (2011) 2199.
[21] M.L. Vestal, Hizrbak if Nass Soectrinetry 44 (2009) 303–317.
[22] V.V. Laiko, N.I. Taranenko, V.D. Berkout, M.A. Yakshin, C.R. Prasad, H. Sang Lee, V.M. Doroshenko, J. Am. Soc. Mass Spectrom. 13 (2002) 354–361.
[23] B. Jenčič, L. Jeromel, N. Ogrinc-Potočnik, K. Vogel-Mikuš, E. Kovačec, M. Regvar, Z. Siketić, P. Vavpetič, Z. Rupnik, K. Bučar, M. Kelemen, J. Kovač, P. Pelicon, Molecular imaging of cannabis leaf tissue with MeV-SIMS method, Nucl. Instrum. Methods Phys. Res. B 371 (2016) 205–210.
[24] L. Jeromel, Development of MeV – SIMS Imaging Mass Spectrometry based on Time of Flight Measurement, Doctoral Thesis, 2015.
[25] P. Vavpetič, K. Vogel-Mikuš, L. Jeromel, N. Ogrinc-Potočnik, P. Pongrac, D. Drobne, Ž. Pipan Tkalec, S. Novak, M. Kos, Š. Koren, M. Regvar, P. Pelicon, Elemental distribution and sample integrity comparison of freeze-dried and frozen-hydrated biological tissue samples with nuclear microprobe, Nucl. Instrum. Methods Phys. Res. B 348 (2015) 147–151.
[26] A. Detterbeck, P. Pongrac, S. Rensch, S. Reuscher, M. Pečovnik, P. Vavpetič, P. Pelicon, S. Holzheu, U. Kraemer, S. Clemens, Spatially resolved analysis of variation in barley (Hordeum vulgare) grain micronutrient accumulation, New Phytol. 211 (2016) 1241–1254.
[27] P. Vavpetič, P. Pelicon, K. Vogel-Mikuš, N. Grlj, P. Pongrac, L. Jeromel, N. Ogrinc-Potočnik, M. Regvar, Micro-PIXE on thin plant tissue samples in frozen hydrated state: a novel addition to JSI nuclear microprobe, Nucl. Instrum. Methods Phys. Res. B 306 (2013) 140–143.
[28] P. Pelicon, N.C. Podaru, P. Vavpetič, L. Jeromel, N. Ogrinc Potičnik, S. Ondračka, A. Gottdang, D.M. Mous, A high brightness proton injector for the Tandetron accelerator at Jožef Stefan Institute, Nucl. Instrum. Methods Phys. Res. B 332 (2014) 229–233.
[29] K.J. Cloete, B. Jenčič, Ž. Šmit, M. Kelemen, K. Mkentanee, P. Pelicon, Detection of lithium in scalp hair by time-of-flight secondary ion mass spectrometry with high energy (MeV) primary ions, Analyt. Methods 9 (2017) 5249–5253.
[30] R.E. Johnson, Electronic sputtering: from atomic physics to continuum mechanics, Phys. Today 36 (1992) 28–36.
[31] J. Simčič, P. Pelicon, M. Budnar, Ž. Šmit, The performance of the Ljubljana ion microprobe, Nucl. Instrum. Methods Phys. Res. B 190 (2002) 283–286.
[32] J. Aoki, M. Toyoda, Development of stigmatic time-of-flight imaging mass spectrometer, J. Mass. Spec. Japan 61 (3) (2013) 23–33.
[33] H. Hazama, J. Aoki, H. Nagao, R. Suzuki, T. Tashima, K. Fujii, K. Masuda, K. Awazu, M. Toyoda, Y. Naito, Construction of a novel stigmatic MALDI imaging mass spectrometer, Appl. Surf. Sci. 255 (4) (2008) 1257–1263.
[34] X. Llopart, R. Ballabriga, M. Campbell, L. Tlustos, W. Wong, Nucl. Instrum. Methods Phys. Res. A 581 (2007) 485.
[35] S. Syed, G.B. Eijkel, P. Kistemaker, S. Ellis, S. Maher, D.F. Smith, R.M. Heeren, Anal. Bioanal. Chem. 407 (8) (2015) 2055–2062.
[36] A. Kiss, J.H. Jungmann, D.F. Smith, R.A. Heeren, Microscope mode secondary ion mass spectrometry imaging with a Timepix detector, Rev. Sci. Instrum. 84 (2013) 013704.
[37] J.H. Jungmann, D.F. Smith, L. MacAleese, I. Klinkert, J. Visser, R.M. Heeren, Biological tissue imaging with a position and time sensitive pixelated detector, J. Am. Soc. Mass Spec. 23 (10) (2012) 1679–1688.
[38] S.R. Ellis, J.H. Jungmann, D.F. Smith, J. Soltwisch, R.M. Heeren, Enhanced detection of high-mass proteins by using an active pixel detector, Angew. Chem. 52 (2013) 11261–11264.